Chemical Science

ROYAL SOCIETY OF CHEMISTRY

EDGE ARTICLE

View Article Online
View Journal | View Issue

Cite this: *Chem. Sci.*, 2020, **11**, 2707

All publication charges for this article have been paid for by the Royal Society of Chemistry

Received 11th November 2019
Accepted 31st January 2020

DOI: 10.1039/c9sc05698j

rsc.li/chemical-science

n → π* interactions as a versatile tool for controlling dynamic imine chemistry in both organic and aqueous media†

Hang Chen,‡[ab] Hebo Ye,‡[a] Yu Hai,[ab] Ling Zhang[a] and Lei You *[ab]

The imine bond holds a prominent place in supramolecular chemistry and materials science, and one issue is the stability of imines due to their electrophilic nature. Here we introduced *ortho*-carboxylate groups into a series of aromatic aldehydes/imines for dictating imine dynamic covalent chemistry (DCC) through n → π* interactions, one class of widespread and yet underused non-covalent interactions. The thermodynamically stabilizing role of carboxylate-aldehyde/imine n → π* interactions in acetonitrile was elucidated by the movement of the imine exchange equilibrium and further supported by crystal analysis. Computational studies provided mechanistic insights for n → π* interactions, the strength of which can surpass that of CH hydrogen bonding and is dependent on the orientation of interacting sites based on natural bond orbital analysis. Moreover, the substituent effect and the combination of recognition sites allowed additional means for modulation. Finally, to show the relevance of our findings *ortho*-carboxylate containing aldehydes were used to regulate imine formation/exchange in water, and modification of the N-terminus of amino acids and peptides was achieved in a neutral buffer. This work represents the latest example of weak interactions governing DCC and sets the stage for assembly and application studies.

Introduction

The imine bond plays a notable role in supramolecular and dynamic covalent chemistry (DCC) as well as materials science.[1–3] By rendering classical covalent bonds reversible, the field of DCC has been flourishing over the past decade.[4–6] Among the most explored dynamic covalent reactions (DCRs) imine formation and exchange have been widely used for the assembly of discrete structures, such as macrocycles, cages, and knots.[7–10] The scrambling of components between imine assemblies also offers many possibilities toward complex systems, including molecular machinery, self-healing systems, signaling networks, and biomimic interfaces.[11–16] In addition, the imine linkage holds a paramount position in the rapid development of covalent organic frameworks, which have found utility in storage, separation, sensing, and catalysis.[17–20] Furthermore, as an inherent reactive site in peptides/proteins the amine group provides a handle for the labeling of biomolecules and ensuing regulation.[21–23]

Although many advances have been made in imine chemistry, one issue is the stability and thus robustness of the imine bond due to the electrophilic nature.[24,25] This problem is further exacerbated in aqueous solution, the working medium of nature.[21–23] The post-structural modification, such as the reduction of the imine bond, helps assuage the stability issue at the cost of reversibility.[26] Despite the enhanced stability of hydrazone/oxime, their formation and exchange generally requires acid or nucleophilic catalysis.[27–30] By taking a page from "neighboring group participation" in organic chemistry, adjacent recognition sites were used to control the imine. For example, salicylaldehyde derived imine (*i.e.*, *ortho*-hydroxyl) is stabilized through enamine/imine tautomerization and resonance-assisted hydrogen bonding (Fig. 1a).[31–34] For another important building block, pyridine-2-carboxaldehyde and its derivatives, their imine assemblies were often constructed with metal coordination (Fig. 1b).[35–37] Moreover, an *ortho*-boronic acid unit was employed to modulate imine and hydrazone through B–N dative bonds (Fig. 1c).[38–41] Such interplay between reversible covalent and supramolecular reactivity has been opening up ample opportunities ranging from dynamic assemblies and complex systems to functionalization.

As one class of underrated non-covalent interactions, orbital donor–acceptor interactions, such as n → π* interactions, have generated significant interest recently, as they are closely associated with molecular recognition, catalysis, and organic materials.[42–49] The overlapping of the lone pair (*n*) and the π* orbital, along the Bürgi–Dunitz trajectory of a nucleophile

[a]*State Key Laboratory of Structural Chemistry, Fujian Institute of Research on the Structure of Matter, Chinese Academy of Sciences, Fuzhou 350002, China. E-mail: lyou@fjirsm.ac.cn*

[b]*University of Chinese Academy of Sciences, Beijing 100049, China*

† Electronic supplementary information (ESI) available: Experimental details, X-ray data, NMR and mass spectra, and DFT calculations. CCDC 1964753 and 1964754. For ESI and crystallographic data in CIF or other electronic format see DOI: 10.1039/c9sc05698j

‡ These authors contributed equally to this work.

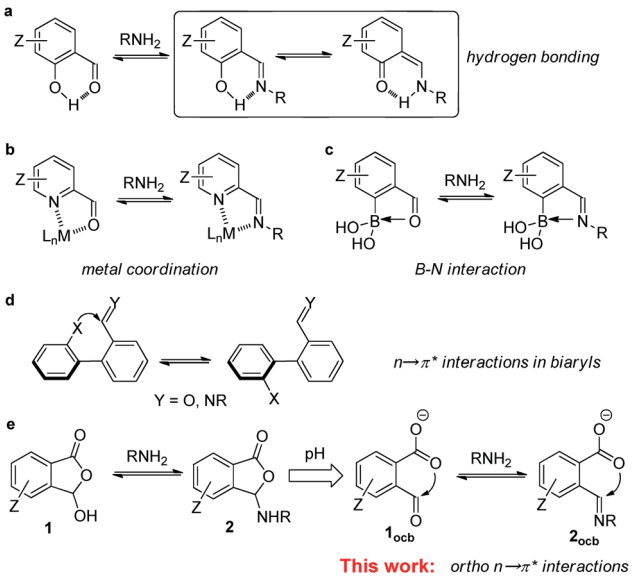

Fig. 1 Neighboring supramolecular recognition sites for dictating imine chemistry. (a) Hydrogen bond with salicylaldehyde. (b) Metal coordination with pyridine-2-carboxaldehyde. (c) B–N dative bond with 2-formylphenylboronic acid. (d) n → π* interaction at the 2,2′ positions of biaryl. (e) The current work of *ortho* n → π* interaction with 2-formylbenzoic acid derivatives.

approaching an electrophile, can result in the delocalization of electron density and thus stabilization.[50,51] A large amount of effort has been devoted to the elucidation of the effect of carbonyl–carbonyl n → π* interactions on the structure, stability, and reactivity of peptides/proteins and their analogs.[42,52–56] In addition to orbital interaction it was revealed that electrostatic interaction in terms of π-hole based carbon bonding contributes to lone pair-carbonyl interactions.[57,58] As compared to the increasing popularity of halogen/chalcogen bonding[59–63] and anion–π interactions,[64–69] the use of n → π* interactions for regulating synthetic systems still remains scarce. It is thus imperative to diversify the molecules manifesting n → π* interactions and to further uncover new building units and regulating mechanisms.

Stimulated by the aforementioned neighboring effect, we wondered about the possible role of *ortho* n → π* interaction in imine DCC (Fig. 1e). In contrast to the supramolecular interactions in Fig. 1a–c, wherein aldehyde oxygen/imine nitrogen servers as an electron donor, we sought an interacting mode with aldehyde/imine carbon as an electron acceptor. The *ortho*-recognition sites also have the advantage of inherent adjacency, different from n → π* interactions at the 2,2′ position of biphenyls wherein conformational equilibrium can switch the interaction on and off (Fig. 1d).[70–72] In the current work a suite of *ortho*-carboxyl aromatic aldehydes (**1**, Fig. 1e) and associated imines (**2**) allowed an in-depth evaluation of weak interactions dictating their reactivity and stability. The carboxylate-aldehyde/imine n → π* interactions provided stabilizing forces for anionic open aldehyde/imine in acetonitrile and resulted in the shift of the imine exchange equilibrium. Moreover, the critical role of n → π* interactions, including the interplay with CH hydrogen bonding, the regulation through the substituent effect, and the combination with different recognition motifs, was confirmed through a collection of experimental and computational evidence. Finally, to demonstrate the utility, aldehydes with *ortho*-carboxylate were employed for imine formation/exchange in water, and labeling of the N-terminus of amino acids and peptides was further achieved in a neutral buffer. These results established spatial orbital interaction as a valuable tool for controlling DCC and set the scene for assembly and functionalization endeavors.

Results and discussion

Hypothesis and design

2-Formylbenzoic acid exists in the ring form (**1**, Fig. 1e),[73–76] with ring/chain tautomerization further dependent on imine formation (**2**, Fig. 1e). To our surprise, non-covalent interactions within 2-formylbenzoic acid and its analogs have escaped from attention. Open aldehyde/imine was thus mainly focused on to elucidate participating weak interactions, as base induced ring opening would afford the conjugate base form ($\mathbf{1_{ocb}}$ and $\mathbf{2_{ocb}}$). More importantly, we postulated that the incorporation of a donating carboxylate group at the *ortho* position of an arylaldehyde and its imine would stabilize the C=Y (Y = O, NR) bond through carboxylate/C=Y n → π* interaction (Fig. 1e). In addition, DCRs of **1** with amines to create **2** would perturb the system in response to the change in electrophilicity from the aldehyde to its imine. Furthermore, the ionization of the carboxyl group to give carboxylate would offer us the opportunity to enhance the solubility of aldehyde **1**/imine **2** and also to exert control on n → π* interactions and imine DCC in water. It is also worthwhile to mention that hydrogen bonding between aldehyde/imine CH and carboxyl oxygen (CH···O) could affect n → π* interactions (C···O) as they share the oxygen donor.

To systematically examine the role of the *ortho*-carboxyl unit, a series of aromatic aldehydes with varied substituents was prepared (**1a–1e**, Fig. 2a). The derivatives of pyridine-2-carboxaldehyde (**1f**) and salicylaldehyde (**1g**) were also studied to probe potential cooperative effects from additional recognition sites. The parent aldehydes (**3a–3g**) and their imines (**4a–4g**) were employed as controls (Fig. 2a). By taking advantage of the reversibility of DCC systems, the thermodynamic effect of adjacent recognition sites, such as carboxyl, could be measured with *in situ* competing target and reference DCRs in one vessel (Fig. 2b). The free energy difference (ΔG_{ex}) of the imine exchange equilibrium would be directly reflective of the relative affinity of aldehydes toward amines ($\Delta G_1 - \Delta G_2$), thus providing a facile method for quantification.[77–79] In essence, the movement of the imine exchange equilibrium would provide an estimation of participating weak interactions.

Imine formation and exchange in acetonitrile

The reaction of **1d** (a of Fig. 2A) with 1-butylamine in CD_3CN afforded the desired product quickly in a nearly quantitative yield (Fig. S3†). A resonance around 6.6 ppm emerged, indicative of the creation of the cyclic hemiaminal ether **2d** (b of

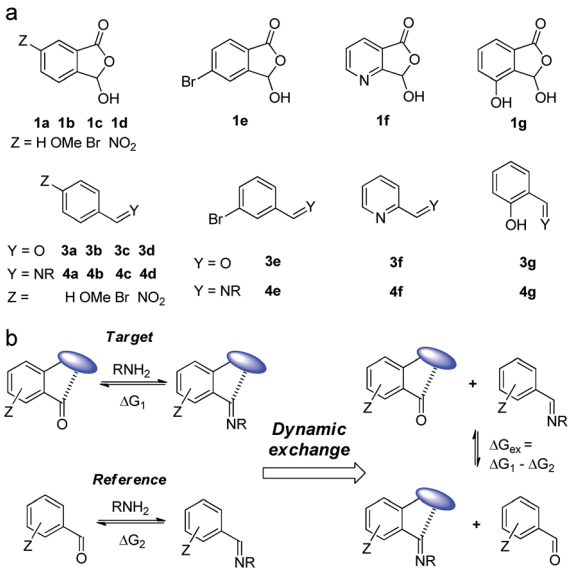

Fig. 2 (a) Compounds (**1**) and controls (**3** and **4**) studied in this work. (b) Dynamic component exchange for probing the thermodynamic effect of nearby recognition sites (represented by the blue oval) on imine DCC.

Fig. 2A). The domination of ring tautomers was also found in **1a–1f** (Fig. S1†) as well as their corresponding amine adducts **2a–2f** (Fig. S4–S15†). The anionic open forms were created by simply titrating the base DBU into **1**/**2** (Fig. S18–S26†) or performing DCRs with amines with DBU present (Fig. S27–S33†). Taking **1d** as an example, the emergence of a peak at 10.8 pm with 1.2 equiv. of DBU (a of Fig. 3B) suggested the formation of the conjugate base of the aldehyde form ($\mathbf{1d_{ocb}}$). Base promoted ring opening was also observed with **2d**, giving anionic imine $\mathbf{2d_{ocb}}$ (b of Fig. 3B). The open imine was detected for **2g** even without the base, as evidenced by the appearance of imine CH at 8.9 ppm (Fig. S16†). The unique behavior of **2g** was explained with the stabilizing role of enamine/imine tautomerization and hydrogen bonding for salicylaldehyde derived imine (Fig. 1a).

In order to probe the existence of n → π* interaction, aldehyde exchange was next conducted in CD_3CN (Fig. 3). The competition between arylaldehyde (**3**) and its *ortho*-carboxyl derivative (**1**) for the reaction with 1-butylamine was examined (exchange 1 and 2). In the absence of DBU (Fig. 3A) amine assemblies incorporating a carboxyl (**2**) were favored in all cases ($K_1 > 1$, Fig. 3C and S34–S41†). For example, the largest K_1 value of 59.7 was obtained, overwhelmingly preferring **2b** over **4b** (*p*-OMe). A K_1 value of 44.7, 14.3, and 3.90 was found for H (**1a**), *p*-Br (**1c**), and *p*-NO_2 (**1d**), respectively (c of Fig. 3A). The smallest K_1 (1.27) for **1g** is consistent with the aforementioned effect of the salicylaldehyde motif. We interpreted the higher affinity of **1** toward amines with the stabilization of the lactone form of **2** (a of Fig. 3D) through the anomeric effect[80,81] on hemiaminal ether carbon arising from overlapping between the lone pair of the nitrogen atom and σ* orbital of the C–O bond (n → σ*(C–O)

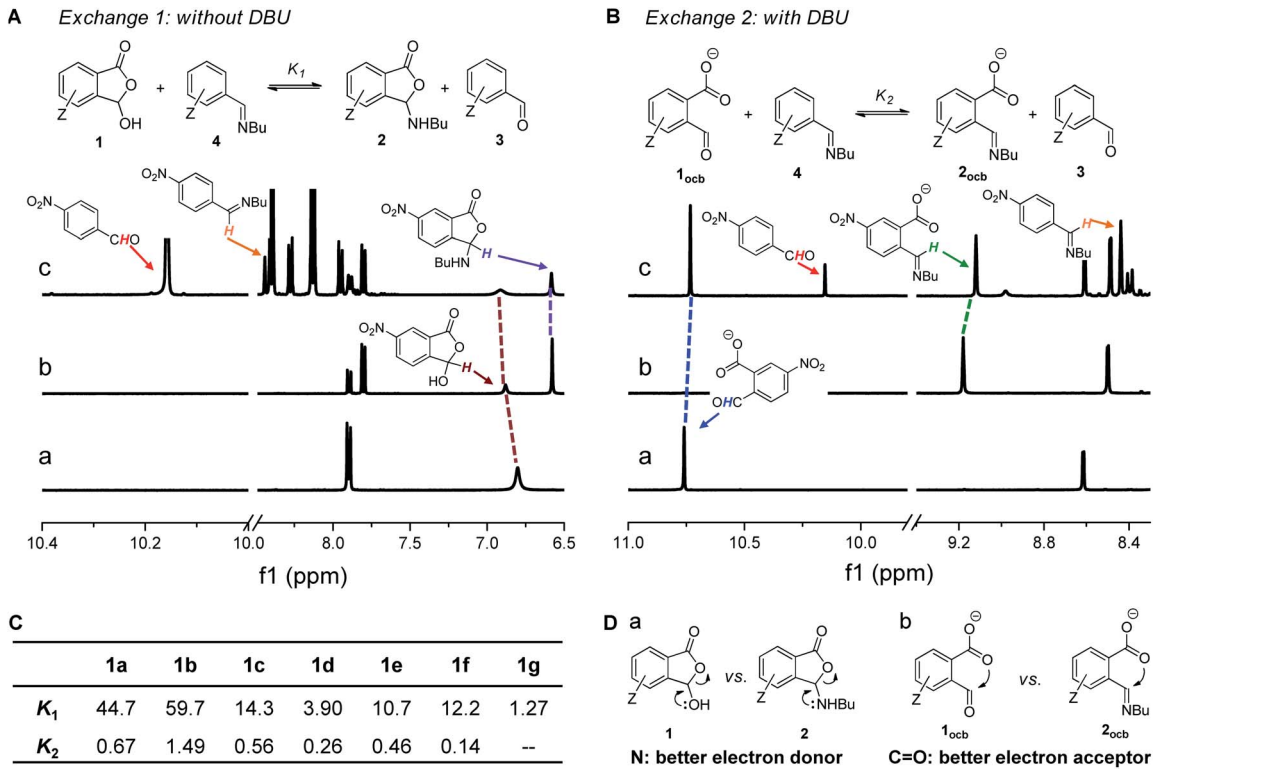

C

	1a	1b	1c	1d	1e	1f	1g
K_1	44.7	59.7	14.3	3.90	10.7	12.2	1.27
K_2	0.67	1.49	0.56	0.26	0.46	0.14	--

Fig. 3 (A) Imine exchange 1 between **1** and **4**, with ^{1}H NMR spectra of **1d** (a), **2d** (b), and exchange (c) shown. (B) Imine exchange 2 between $\mathbf{1_{ocb}}$ and **4** in the presence of DBU, with ^{1}H NMR spectra of $\mathbf{1d_{ocb}}$ (a), $\mathbf{2d_{ocb}}$ (b), and exchange (c) shown. (C) Summary of equilibrium constants for imine exchanges **1** and **2**. (D) Illustration of the stabilizing effect of *ortho*-carboxyl (a) and carboxylate (b) on cyclic and open aldehyde/imine, respectively. Solvent: CD_3CN.

interaction). Due to nitrogen being a better electron donor than oxygen, such an effect would be more dominant in **2** than **1**.

Interestingly, there was a sharp decrease in the equilibrium constant of imine exchange (Fig. 3B) when DBU (1.2 equiv.) was added into the mixture of **1**, **3**, and 1-butylamine to form anionic open aldehyde $\mathbf{1}_{ocb}$ and imine $\mathbf{2}_{ocb}$ (K_2, Fig. 3C and S42–S48†). For example, the base enabled the reversal of the position of the equilibrium for *p*-NO_2, with aldehyde $\mathbf{1d}_{ocb}$ favored (K_2 = 0.26, c of Fig. 3B). **1a** (H), **1b** (*p*-OMe), and **1c** (*p*-Br) gave a K_2 value of 0.67, 1.49, and 0.56, respectively, all of which are significantly smaller than K_1. The smallest K_2 (0.14) was found with **1f**. These findings were rationalized as follows: since open aldehydes are more electron-deficient and thus better electron acceptors than their imines, through-space carboxylate-aldehyde n → π* interaction would become stronger than that of imine, resulting in enhanced stabilization and accumulation of aldehyde $\mathbf{1}_{ocb}$ (b of Fig. 3D). As a result, the thermodynamic effect of neighboring carboxyl can be readily modulated *via* changing the pH.

To further isolate the role of n → π* interaction from the electronic effect of carboxylate, analogous exchange reactions were run by using *meta*- and *para*-carboxylate-benzaldehyde ($\mathbf{1a}_{ocb}$ (*meta*) and $\mathbf{1a}_{ocb}$ (*para*)), respectively (Fig. S49 and S50†). The carboxylate at the *meta* or *para* position is unlikely to interact directly with aldehyde and its imine but could influence them through the electronic effect. $\mathbf{1a}_{ocb}$ (*meta*) and $\mathbf{1a}_{ocb}$ (*para*) afforded K_2 values of 2.01 and 1.65, different from the data of $\mathbf{1a}_{ocb}$ (0.67). These results support the shift of the exchange equilibrium through *ortho* n → π* interaction, while *meta*/*para* carboxylate mainly serves as an electron-withdrawing group.

Crystal structures

The next goal was to reveal structural features of associated n → π* interactions. For example, in $\mathbf{1a}_{ocb}$ the aldehyde and carboxylate adopt a torsion angle of 17 and 32° relative to the benzene plane, respectively (Fig. 4a).[82] Such an orientation would be able to accommodate the orbital interaction. A distance of 2.88 Å was revealed between carboxylate oxygen and aldehyde carbon (O···C), further suggesting an attractive interaction. In the X-ray structure of imine $\mathbf{2a}_{ocb}$ a torsion angle of 37 and 11° was found for imine and carboxylate, respectively, which also have close contact (2.79 Å for O···C, Fig. 4b). In addition, hydrogen bonds were found in the crystal packing, such as the one between imine nitrogen and ammonium NH. For pyridine derived imine $\mathbf{2f}_{ocb}$, the co-planarity of C=N with the pyridine plane was apparent, likely facilitated by a hydrogen bonding-bridged five-membered ring (Fig. 4c). Moreover, the carboxylate is significantly twisted (53°) in order to align with the imine carbon (3.00 Å for O···C). The structural parameters, in particular the torsion angles of and the distance between aldehyde/imine and carboxylate, provided further evidence for n → π* interactions.

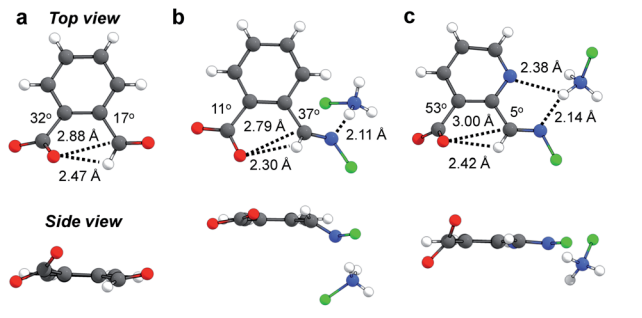

Fig. 4 Crystal structures of $\mathbf{1a}_{ocb}$ (a), $\mathbf{2a}_{ocb}$ (b), and $\mathbf{2f}_{ocb}$ (c). For clarity the cyclohexyl group on the amine nitrogen is shown with a green sphere. The absolute value of the acute angle was used to reflect the torsion angle of carboxylate, aldehyde, or imine relative to the phenyl plane.

Calculations of orbital interactions

DFT calculations were then conducted to offer more insights. The functional/basis set of M06-2X-D3/def2-TZVP was employed, and the PCM solvent model was applied for acetonitrile. The conformer of open conjugate base $\mathbf{1a}_{ocb}$ with the n → π* interaction is dominant (99%, Fig. 5a and S51†), consistent with the X-ray structure. An analogous structure was also obtained for $\mathbf{2a}_{ocb}$ (99%) as for $\mathbf{1a}_{ocb}$ (Fig. 5b and S51†). The alignment of orbitals was further visualized through natural bond orbital (NBO) analysis, which offers an estimation of the interaction energy according to second-order perturbation theory ($\Delta E^{(2)}$).[83] For example, the overlap of two oxygen lone pairs and the antibonding orbital of aldehyde was apparent within $\mathbf{1a}_{ocb}$, with NBO energies of 1.90 and 0.39 kcal mol^{-1}, respectively (Fig. 5a). The sum (2.29 kcal mol^{-1}) was used for analysis here, and a NBO energy of 1.32 kcal mol^{-1} (sum of 1.04 and 0.28 kcal mol^{-1}) was found for carboxylate-imine n → π* interaction in $\mathbf{2a}_{ocb}$ (Fig. 5b). In addition, NBO analysis revealed an n → σ*(CH) stabilization energy of 0.03 kcal mol^{-1} for the CH···O hydrogen bond in $\mathbf{1a}_{ocb}$ (Table S2†), significantly smaller than the corresponding value for n → π* interaction

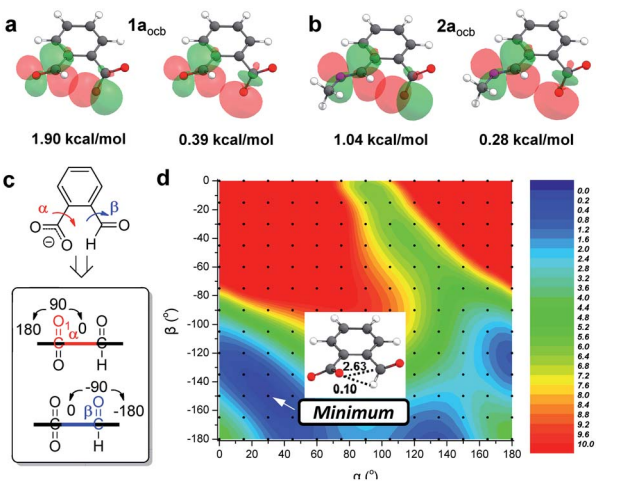

Fig. 5 Optimized structures of open conjugate base (a) $\mathbf{1a}_{ocb}$ and (b) $\mathbf{2a}_{ocb}$, with NBOs and energies listed. (c) Illustration of the torsion scan and definition of α and β. (d) A heat map of the energies of $\mathbf{1a}_{ocb}$ (in kcal mol^{-1}) *versus* (α, β) coordinates. The structure at the minimum and associated NBO energies (n → π* interaction and CH hydrogen bond, in kcal mol^{-1}) are shown.

(2.29 kcal mol^{-1}). A similar trend was found with open imine **2a$_{ocb}$**, preferring n → π* interaction over the CH hydrogen bond. Moreover, the molecular electrostatic potential (MEP) maps of **1a$_{ocb}$** and **2a$_{ocb}$** were calculated, and the attractive interaction between the electron-rich region of carboxylate oxygen and electron-deficient region of aldehyde/imine carbon was apparent as compared to the donor (carboxylate) and acceptor (aldehyde/imine) fragments (Fig. S52†). These results are consistent with the contribution of both orbital and electrostatic interactions for lone pair-carbonyl contacts.

To further elaborate the extent of weak interactions, a rigid potential energy surface scan of **1a$_{ocb}$** was performed. The orientation of carboxylate (α) and aldehyde (β) relative to the phenyl plane was varied (Fig. 5c), and the minimized energies of ensuing rotamers are shown in a heat plot (Fig. 5d). The most stable isomer was found at (30°, −150°) in the blue region, echoing the X-ray (α = 32°, β = −163°) as well as geometry-optimized (α = 29°, β = −156°) structures of **1a$_{ocb}$**. The n → π* interaction (2.63 kcal mol^{-1}) was dominant compared to CH···O hydrogen bonding (0.10 kcal mol^{-1}). Moreover, low-energy blue regions along the α and β axes were identified. In addition, there are two red regions (upper left and upper right) with overwhelmingly unfavorable energies due to strong electronic repulsion between carboxylate oxygen and aldehyde oxygen. The loss of conjugation of aldehyde and carboxylate with the aromatic ring at (90°, −90°) seriously undermines the stability (9.7 kcal mol^{-1}). Nevertheless, a planar isomer at (0°, −180°) or (180°, −180°) is also unfavorable (4.5 kcal mol^{-1}), as n → π* interaction can't contribute since the carboxylate resides on the nodal plane of the π* orbital of the carbonyl. Torsion scan analysis of **2a$_{ocb}$** also verified its optimized structure (Fig. S53†). Overall, we interpreted these results as follows: to accommodate the alignment of orbitals and thus directionality of n → π* interaction and concomitantly to compensate the energy change as a result of varying conjugation, the torsion angle of aldehyde (α) and carboxylate (β) would be adaptive.

Substituent effects on n → π* interactions

With weak interactions governing aldehyde **1a$_{ocb}$**/imine **2a$_{ocb}$** elucidated, substituent effects were further examined as a means of regulating n → π* interactions (Fig. 6). The major structures of the open conjugate base forms for a suite of *ortho*-carboxylate aldehydes and imines (**1$_{ocb}$** and **2$_{ocb}$**) were calculated (Table S2†), and NBO stabilization energies of n → π* interactions were summarized (Fig. 6a). In general a larger NBO value was found for aldehyde than for its associated imine, supporting the explanation in Fig. 3. Among *para* or *meta*-substituted aldehydes **1d$_{ocb}$** (*p*-NO$_2$) gave the strongest n → π* interaction (4.49 kcal mol^{-1}), while **1b$_{ocb}$** (*p*-OMe) had the weakest (0.72 kcal mol^{-1}). The data for **1a$_{ocb}$** (H), **1c$_{ocb}$** (*p*-Br) and **1e$_{ocb}$** (*m*-Br) fell in the middle. A similar trend was found for imine **2**, though the discrimination between substituents is modest. The sequence of NBO data largely falls in line with the electron-withdrawing ability of the *para*-substituent. Electron-donating *p*-OMe can stabilize the aldehyde/imine *via* the resonance effect, hence decreasing the electrophilicity and in turn weakening the n → π* interactions.

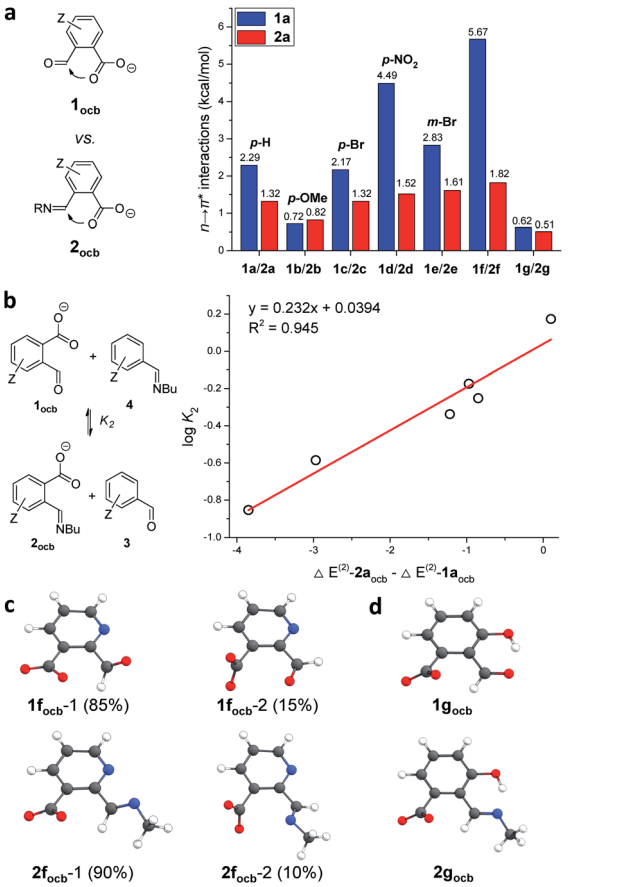

Fig. 6 (a) Comparison of NBO energies of n → π* interactions in **1$_{ocb}$** and **2$_{ocb}$**. (b) Correlation of log K_2 with the difference in n → π* NBO energies of **1a$_{ocb}$** and **2a$_{ocb}$**. Optimized structures and populations of isomers of **1f$_{ocb}$** and **2f$_{ocb}$** (c), as well as **1g$_{ocb}$** and **2g$_{ocb}$** (d).

The interplay of n → π* interactions with other recognition motifs was then probed. For **1f$_{ocb}$** besides isomer **1f$_{ocb}$-1** (85%) **1f$_{ocb}$-2** accounted for 15% of the population (Fig. 6c). The decreased percentage of **1f$_{ocb}$-1** over **1a$_{ocb}$** (99%) is likely due to the electronic repulsion between pyridine nitrogen and carbonyl oxygen in **1f$_{ocb}$-1**. Similar results were also revealed with **2f$_{ocb}$** (Fig. 6c). The NBO energy of n → π* interactions is significant for **1f$_{ocb}$-1** (5.67 kcal mol^{-1}) and **2f$_{ocb}$-1** (1.82 kcal mol^{-1}, Fig. 6a). The enhancement of NBO energies of n → π* interactions in **1f$_{ocb}$-1** and **2f$_{ocb}$-1** as compared to **1a$_{ocb}$** and **2a$_{ocb}$** (2.29 and 1.32 kcal mol^{-1}) can be attributed to the electron-withdrawing ability of pyridine. One conformer was dominant for **1g$_{ocb}$** and **2g$_{ocb}$** (Fig. 6d), as in the case of **1a$_{ocb}$** and **2a$_{ocb}$**. Moreover, NBO analysis revealed an n → π* interaction energy of 0.62 and 0.51 kcal mol^{-1} for **1g$_{ocb}$** and **2g$_{ocb}$**, respectively (Fig. 6a). These values are significantly smaller than the data for **1a$_{ocb}$** and **2a$_{ocb}$**. Hydrogen-bonding facilitated aldehyde/enol and imine/enamine tautomerization[23] in the open forms of **1g** and **2g** would reduce the electrophilicity of aldehyde and imine, accordingly attenuating their corresponding orbital interactions with nearby carboxyl groups.

Nevertheless, the contribution arising from neighboring carboxyl to the overall reaction is still significant, as revealed by imine exchanges with **1f**/**1g** in Fig. 4. More importantly, a linear correlation of log *K* of exchange 2 with the difference in n → π* interaction energies of aldehydes $\mathbf{1}_{ocb}$ and imines $\mathbf{2}_{ocb}$ was obtained, further validating their contribution (Fig. 6b and Table S3†).

Imine DCC in aqueous solutions

Having gathered both experimental and theoretical evidence for n → π* interactions, the control of imine DCC in water was further explored. There is intensive interest in supramolecular and dynamic covalent chemistry in water, the environment of nature.[84–86] Gratifyingly, the creation of open imines was found for the reactions of **1a–1g** with ethanolamine (2.0 equiv.) in D_2O (Fig. S54–S60†), as an excess amount of amine deprotonated the carboxyl to solubilize aldehyde **1** and imine **2** in the form of their anionic conjugate bases ($\mathbf{1}_{ocb}$ and $\mathbf{2}_{ocb}$). To gauge the thermodynamic effect of *ortho* carboxylate, the competition between **1** and **3** for reactions with ethanolamine (2.0 equiv.) was then examined in D_2O (with 10% DMSO-d_6, exchange 3 in Fig. 7a). Imine **2** was preferred in all cases ($K_3 > 1$), supporting the shift of the imine exchange equilibrium toward the right (Fig. 7a and S61–S67†). A *K* value of 3.30 and 3.10 was revealed for **1f** and **1g**, respectively, while **1a–1e** gave a *K* value around 1.30. Relative to acetonitrile different equilibrium constants were obtained in aqueous solution. To further probe solvent effects, exchange reactions between **1a** and **4a** were run in different solvent mixtures (Fig. S70–S77, Table S4†). Upon increasing the percentage of water there was an enhancement in the *K* value, indicating gradual movement of the equilibrium toward the right. One explanation comes from the stabilization of imine **2** *via* hydrogen bonding with water in conjunction with n → π* interaction, and the different capability of forming hydrogen bonds between aldehyde oxygen and imine nitrogen with water would modulate corresponding n → π* interactions. Hydrogen bond and n → π* interaction working collectively to modulate the system have been reported.[42,52,70]

Aldehydes **1f** and **1g** were further studied as they gave larger K_3 values than others. A series of aldehyde exchanges with **1a** as a reference was also conducted to identify the aldehyde exhibiting the best affinity for ethanolamine (3.0 equiv., exchange 4 in Fig. 7a and S78–S83†). Salicylaldehyde derived **1g** gave the largest *K* value (46.9), strongly preferring its imine **2g** (Fig. 7a). A *K* value of 21.3 was obtained with pyridine derived **1f**. The enhanced affinity of **1f** and **1g** toward the amine is rationalized with stabilizing forces arising from nearby recognition sites of pyridine nitrogen or phenol along with n → π* interaction. DFT calculation of model compounds corroborated the hypothesis. Water bridged concerted hydrogen bonds were apparent, with n → π* NBO energies of 4.52 and 1.84 kcal mol^{-1} for **1f** and **2f**, respectively (Fig. 7b). With **1f** there was a decrease in NBO data (4.52 kcal mol^{-1}) of orbital interaction in water as compared to acetonitrile (5.67 kcal mol^{-1}, Fig. 6a), suggesting that concerted hydrogen bonding with water attenuates n → π* interaction in **1f**. However, the n → π* NBO value for **2f** remained nearly the same between water (1.84 kcal mol^{-1}) and acetonitrile (1.82 kcal mol^{-1}). These trends explain the reversal in the equilibrium constant from acetonitrile (0.14) to water (3.30) for **1f**. Phenol mediated intramolecular hydrogen bonds were found for **1g** and **2g**, which afforded n → π* NBO energies of 0.61 and 0.52 kcal mol^{-1}, respectively (Fig. 7c). These values are similar to the data for acetonitrile, and n → π* interaction is weakened due to intramolecular hydrogen bonding. Although hydrogen bonding would play a dominant role in stabilizing imines **2f** and **2g**, *ortho* carboxylate still contributes, as reflected by a K_3 value of 3.30 and 3.10 for **2f** and **2g**, respectively. These results indicate the feasibility of the combination of different recognition sites for modulating imine chemistry.

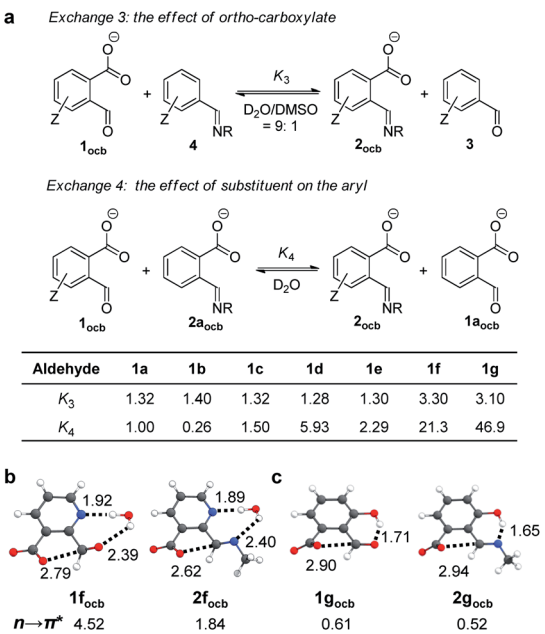

Aldehyde	1a	1b	1c	1d	1e	1f	1g
K_3	1.32	1.40	1.32	1.28	1.30	3.30	3.10
K_4	1.00	0.26	1.50	5.93	2.29	21.3	46.9

Fig. 7 (a) Imine exchange 3 between between **1** and **4** in D_2O : DMSO-d_6 (9 : 1) as well as imine exchange 4 between **1** and **2a** in D_2O, with equilibrium constants listed. Optimized structures of $\mathbf{1f}_{ocb}$ and $\mathbf{2f}_{ocb}$ (b), as well as $\mathbf{1g}_{ocb}$ and $\mathbf{2g}_{ocb}$ (c), with distances (Å) and NBO energies (kcal mol^{-1}) of n → π* interactions shown.

Imine DCC at physiological pH

Encouraged by the findings in water, imine formation and exchange were then studied at physiological pH. Aldehyde **1g** was chosen as it gave the largest *K* for exchange 4. A *K* value of 2.90 was afforded for the competition of **1g** and salicylaldehyde for ethanolamine at pH 7.4 (50 mM PBS buffer), again preferring **2g** (Fig. S84†). The reaction of **1g** (10 mM) with ethanolamine (1.2 equiv.) readily gave imine **2g**, albeit with a modest yield (17%) at pH 7.4 (Fig. S85 and S86†). A slightly smaller yield (12%) was apparent at pH 7.0, while there was an increase in the yield of imine (30%) when the pH was switched to 7.8 (Fig. S87†). Moreover, the yields remained constant after a week (Table S5†). In order to optimize the extent of imine formation in a pH 7.4 buffer, a series of DCRs were performed while

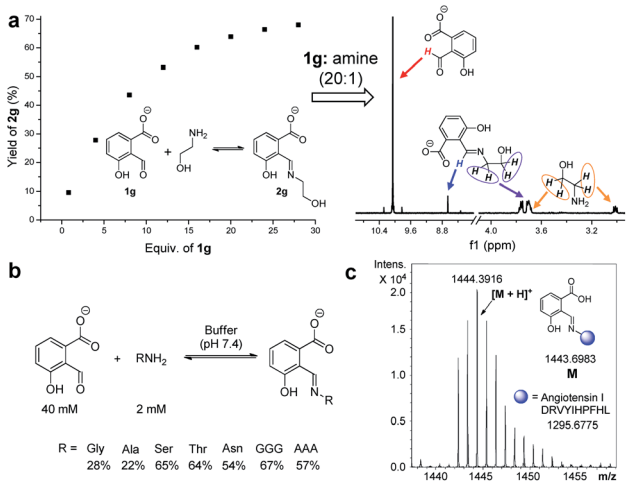

Fig. 8 (a) The yield of the reaction of varied concentrations of **1g** and ethanolamine (2.0 mM) in buffer (pH 7.4), with one ^{1}H NMR spectrum shown. (b) Representative structures and yields of **2g** incorporating amino acids/peptides in the buffer (pH 7.4). (c) ESI-mass spectrum of **2g** incorporating the peptide angiotensin I in the buffer (pH 7.4).

maintaining the concentration of ethanolamine at a constant (2.0 mM) and varying that of **1g**. With an aldehyde/amine ratio around 20, a yield larger than 60% was obtained (Fig. 8a and S88†).

Finally, attention was turned to the modification of biomolecules. As an inherent reactive site in peptides/proteins the amine group provides a handle for bioconjugation.[21,87,88] For example, the reaction of **1g** (40 mM) with amino acids, such as glycine and alanine (2 mM each), afforded the corresponding imine with a yield of 28% and 22% at pH 7.4, respectively (Fig. 8b and S91–S100†). To further check the utility, the modification of several model peptides was examined, such as triglycine, trialanine, and angiotensin I (Fig. 8c). With an aldehyde/peptide ratio of 20 : 1, the desired product was found by ESI mass spectral analysis (Fig. S101–S108†). These results demonstrate potential applications in biological labelling.

Conclusions

In summary, we developed a facile platform for the modulation of dynamic imine chemistry with n → π* interactions. A detailed investigation of imine exchanges with a library of *ortho*-carboxyl aromatic aldehydes was conducted, and n → π* interactions played a stabilizing role in the anionic open aldehyde/imine, leading to the shift of imine exchange equilibrium. Moreover, theoretical calculations, including NBO analysis and torsion scan, provided deep insights for n → π* interactions, which can compete with CH hydrogen bonding and can be modulated by the substituent effect. In addition, the incorporation of *ortho*-carboxyl into salicylaldehyde and pyridine-2-carboxaldehyde demonstrated the feasibility of the use of different recognition sites. Aldehydes with *ortho*-carboxylate were further employed for the regulation of imine formation/exchange in water, and the modification of the N-terminus of amino acids and peptides was realized at neutral pH. The strategy of *ortho*-carboxyl containing aldehydes showcases the capability of even weak interactions, such as orbital interactions, for controlling the DCC, and will open new possibilities in dynamic assemblies. Considering the popularity of carbonyls and their derivatives in organic compounds, we anticipate that the use of n → π* interactions in supramolecular chemistry, catalysis, and functional materials has significant growth prospects.

Conflicts of interest

There are no conflicts to declare.

Acknowledgements

We thank the NSFC (21672214), the Recruitment Program of Global Youth Experts, and the Strategic Priority Research Program (XDB20000000) and the Key Research Program of Frontier Sciences (QYZDB-SSW-SLH030) of the CAS for funding.

Notes and references

1 M. E. Belowich and J. F. Stoddart, *Chem. Soc. Rev.*, 2012, **41**, 2003–2024.
2 Y. Jia and J. Li, *Chem. Rev.*, 2015, **115**, 1597–1621.
3 H. Vardhan, A. Mehta, I. Nath and F. Verpoort, *RSC Adv.*, 2015, **5**, 67011–67030.
4 Y. Jin, C. Yu, R. J. Denman and W. Zhang, *Chem. Soc. Rev.*, 2013, **42**, 6634–6654.
5 S. J. Rowan, S. J. Cantrill, G. R. L. Cousins, J. K. M. Sanders and J. F. Stoddart, *Angew. Chem., Int. Ed.*, 2002, **41**, 898–952.
6 A. Herrmann, *Chem. Soc. Rev.*, 2014, **43**, 1899–1933.
7 T. Hasell and A. I. Cooper, *Nat. Rev. Mater.*, 2016, **1**, 16053.
8 D. Zhang, T. K. Ronson and J. R. Nitschke, *Acc. Chem. Res.*, 2018, **51**, 2423–2436.
9 Y. Liu and Z.-T. Li, *Aust. J. Chem.*, 2013, **66**, 9–22.
10 G. Zhang and M. Mastalerz, *Chem. Soc. Rev.*, 2014, **43**, 1934–1947.
11 A. Wilson, G. Gasparini and S. Matile, *Chem. Soc. Rev.*, 2014, **43**, 1948–1962.
12 A. J. McConnel, C. S. Wood, P. P. Neelakandan and J. R. Nitschke, *Chem. Rev.*, 2015, **115**, 7729–7793.
13 Q. Ji, R. C. Lirag and O. S. Miljanić, *Chem. Soc. Rev.*, 2014, **43**, 1873–1884.
14 J. M. Lehn, *Angew. Chem., Int. Ed.*, 2015, **54**, 3276–3289.
15 J. Li, P. Nowak and S. Otto, *J. Am. Chem. Soc.*, 2013, **135**, 9222–9239.
16 S. Erbas-Cakmak, D. A. Leigh, C. T. McTernan and A. L. Nussbaumer, *Chem. Rev.*, 2015, **115**, 10081–10206.
17 J. L. Segura, M. J. Mancheno and F. Zamora, *Chem. Soc. Rev.*, 2016, **45**, 5635–5671.
18 J. Jiang, Y. Zhao and O. M. Yaghi, *J. Am. Chem. Soc.*, 2016, **138**, 3255–3265.
19 S. Y. Ding and W. Wang, *Chem. Soc. Rev.*, 2013, **42**, 548–568.

20 C. Qian, Q. Y. Qi, G. F. Jiang, F. Z. Cui, Y. Tian and X. Zhao, *J. Am. Chem. Soc.*, 2017, **139**, 6736–6743.
21 O. Boutureira and G. J. L. Bernardes, *Chem. Rev.*, 2015, **115**, 2174–2195.
22 J. M. Gilmore, R. A. Scheck, A. P. Esser-Kahn, N. S. Joshi and M. B. Francis, *Angew. Chem., Int. Ed.*, 2006, **45**, 5307–5311.
23 A. Bandyopadhyay, S. Cambray and J. Gao, *Chem. Sci.*, 2016, **7**, 4589–4593.
24 M. Ciaccia and S. Di Stefano, *Org. Biomol. Chem.*, 2015, **13**, 646–654.
25 P. G. Cozzi, *Chem. Soc. Rev.*, 2004, **33**, 410–421.
26 M. Liu, M. A. Little, K. E. Jelfs, J. T. A. Jones, M. Schmidtmann, S. Y. Chong, T. Hasell and A. I. Cooper, *J. Am. Chem. Soc.*, 2014, **136**, 7583–7586.
27 D. K. Kölmel and E. T. Kool, *Chem. Rev.*, 2017, **117**, 10358–10376.
28 P. Schmidt, C. Stress and D. Gillingham, *Chem. Sci.*, 2015, **6**, 3329–3333.
29 L. Shen, N. Cao, L. Tong, X. Zhang, G. Wu, T. Jiao, Q. Yin, J. Zhu, Y. Pan and H. Li, *Angew. Chem., Int. Ed.*, 2018, **57**, 16486–16490.
30 S. R. Beeren and J. K. M. Sanders, *Chem. Sci.*, 2011, **2**, 1560–1567.
31 C. M. Metzler, A. Cahill and D. E. Metzler, *J. Am. Chem. Soc.*, 1980, **102**, 6075–6082.
32 J. Crugeiras, A. Rios, E. Riveiros and J. P. Richard, *J. Am. Chem. Soc.*, 2009, **131**, 15815–15824.
33 K. W. Bentley and C. Wolf, *J. Am. Chem. Soc.*, 2013, **135**, 12200–12203.
34 M. Zhang, L. Li, Q. Lin, M. Tang, Y. Wu and C. Ke, *J. Am. Chem. Soc.*, 2019, **141**, 5154–5158.
35 J. Holub, G. Vantomme and J. M. Lehn, *J. Am. Chem. Soc.*, 2016, **138**, 11783–11791.
36 R. Lavendomme, T. K. Ronson and J. R. Nitschke, *J. Am. Chem. Soc.*, 2019, **141**, 12147–12158.
37 C. He, Z. Lin, Z. He, C. Duan, C. Xu, Z. Wang and C. Yan, *Angew. Chem., Int. Ed.*, 2008, **47**, 877–881.
38 P. M. S. D. Cal, J. B. Vicente, E. Pires, A. V. Coelho, L. F. Veiros, C. Cordeiro and M. P. Gois, *J. Am. Chem. Soc.*, 2012, **134**, 10299–10305.
39 S. Cambray and J. Gao, *Acc. Chem. Res.*, 2018, **51**, 2198–2206.
40 B. M. Chapin, P. Metola, V. M. Lynch, J. F. Stanton, T. D. James and E. V. Anslyn, *J. Org. Chem.*, 2016, **81**, 8319–8330.
41 B. Akgun and D. G. Hall, *Angew. Chem., Int. Ed.*, 2018, **57**, 2–19.
42 R. W. Newberry and R. T. Raines, *Acc. Chem. Res.*, 2017, **50**, 1838–1846.
43 S. K. Singh and A. Das, *Phys. Chem. Chem. Phys.*, 2015, **17**, 9596–9612.
44 I. W. Windsor, B. Gold and R. T. Raines, *ACS Catal.*, 2019, **9**, 1464–1471.
45 D. J. Schmucker, S. R. Dunbar, T. D. Shepherd and M. A. Bertucci, *J. Phys. Chem. A*, 2019, **123**, 2537–2543.
46 A. Choudhary, K. J. Kamer and R. T. Raines, *J. Org. Chem.*, 2011, **76**, 7933–7937.
47 B. Sahariah and B. K. Sarma, *Chem. Sci.*, 2019, **10**, 909–917.
48 A. Rahim, P. Saha, K. K. Jha, N. Sukumar and B. K. Sarma, *Nat. Commun.*, 2017, **8**, 1–13.
49 J. Echeverría, *Chem. Commun.*, 2018, **54**, 3061–3064.
50 H. B. Bürgi, J. D. Dunitz and E. Shelter, *J. Am. Chem. Soc.*, 1973, **95**, 5065–5067.
51 R. G. Brennan, G. G. Prive, W. J. P. Blonski, F. E. Hruska and M. Sundaralingam, *J. Am. Chem. Soc.*, 1983, **105**, 7737–7742.
52 C. Siebler, R. S. Erdmann and H. Wennemers, *Angew. Chem., Int. Ed.*, 2014, **53**, 10340–10344.
53 C. Fufezan, *Proteins: Struct., Funct., Genet.*, 2010, **78**, 2831–2838.
54 B. C. Gorske, R. C. Nelson, Z. S. Bowden, T. A. Kufe and A. M. Childs, *J. Org. Chem.*, 2013, **78**, 11172–11183.
55 R. W. Newberry, B. VanVeller, I. A. Guzei and R. T. Raines, *J. Am. Chem. Soc.*, 2013, **135**, 7843–7846.
56 J. S. Laursen, J. Engel-Andreasen, P. Fristrup, P. Harris and C. A. Olsen, *J. Am. Chem. Soc.*, 2013, **135**, 2835–2844.
57 J. Echeverría, *Cryst. Growth Des.*, 2018, **18**, 506–512.
58 R. Shukla and D. Chopra, *CrystEngComm*, 2018, **20**, 3308–3312.
59 H. Wang, W. Wang and W. Jin, *Chem. Rev.*, 2016, **1169**, 5072–5104.
60 G. Cavallo, P. Metrangolo, R. Milani, T. Pilati, A. Priimagi, G. Resnati and G. Terraneo, *Chem. Rev.*, 2016, **116**, 2478–2601.
61 R. Gleiter, G. Haberhauer, D. B. Werz, F. Rominger and C. Bleiholder, *Chem. Rev.*, 2018, **118**, 2010–2041.
62 L. C. Gilday, S. W. Robinson, T. A. Barendt, M. J. Langton, B. R. Mullaney and P. D. Beer, *Chem. Rev.*, 2015, **115**, 7118–7195.
63 K. Selvakumar and H. B. Singh, *Chem. Sci.*, 2018, **9**, 7027–7042.
64 M. Giese, M. Albrecht and K. Rissanen, *Chem. Rev.*, 2015, **1151**, 68867–68895.
65 Y. Zhao, Y. CotelleLe, L. Liu, J. López-Andarias, A. Bornhof, M. Akamatsu, N. Sakai and S. Matile, *Acc. Chem. Res.*, 2018, **51**, 2255–2263.
66 M. X. Wang, *Acc. Chem. Res.*, 2011, **45**, 182–195.
67 D. Tuo, W. Liu, X. Wang, X. Wang, Y. Ao, Q. Wang, Z. Li and D. X. Wang, *J. Am. Chem. Soc.*, 2019, **141**, 1118–1125.
68 H. Zeng, P. Liu, G. Feng and F. Huang, *J. Am. Chem. Soc.*, 2019, **141**, 16501–16511.
69 B. Jiang, W. Wang, Y. Zhang, Y. Lu, C. W. Zhang, G. Q. Yin, X. L. Zhao, L. Xu, H. Tan, X. Li, G. X. Jin and H. B. Yang, *Angew. Chem., Int. Ed.*, 2017, **56**, 14438–14442.
70 H. Zheng, H. Ye, X. Yu and L. You, *J. Am. Chem. Soc.*, 2019, **141**, 8825–8833.
71 E. C. Vik, P. Li, P. J. Pellechia and K. D. Shimizu, *J. Am. Chem. Soc.*, 2019, **141**, 16579–16583.
72 G. W. Breton, L. O. Davis, K. L. Martin and T. A. Chambers, *Cryst. Growth Des.*, 2019, **19**, 3895–3904.
73 P. Kovaříček and J. M. Lehn, *Chem.–Eur. J.*, 2015, **21**, 9380–9384.
74 P. Kovaříček, A. C. Meister, K. Flídrová, R. Cabot, K. Kovaříčková and J. M. Lehn, *Chem. Sci.*, 2016, **7**, 3215–3226.

75 E. T. Kool, D. H. Park and P. Crisalli, *J. Am. Chem. Soc.*, 2013, **135**, 17663–17666.
76 J. Liu, X. Wang, C. Zhao, J. Hao, G. Fang and S. Wang, *J. Hazard. Mater.*, 2018, **344**, 220–229.
77 A. G. Santana, E. Jiménez-Moreno, A. M. Gómez, F. Corzana, C. González, G. Jiménez-Oses, J. Jiménez-Barbero and J. L. Asensio, *J. Am. Chem. Soc.*, 2013, **135**, 3347–3350.
78 M. K. Chung, P. S. White, S. J. Lee, M. L. Waters and M. R. Gagné, *J. Am. Chem. Soc.*, 2012, **134**, 11415–11429.
79 M. K. Chung, S. J. Lee, M. L. Waters and M. R. Gagné, *J. Am. Chem. Soc.*, 2012, **134**, 11430–11443.
80 L. Somsák, *Chem. Rev.*, 2001, **101**, 81–135.
81 K. B. Wiberg, W. F. Bailey, K. M. Lambert and Z. D. Stempel, *J. Org. Chem.*, 2018, **83**, 5242–5255.
82 O. Büyükgüngör and M. Odabaşoğlu, *Acta Crystallogr.*, 2006, **62**, 2749–2750.
83 A. E. Reed, L. A. Curtiss and F. Weinhold, *Chem. Rev.*, 1988, **88**, 899–926.
84 S. Ulrich, *Acc. Chem. Res.*, 2019, **52**, 510–519.
85 X. Sun and T. D. James, *Chem. Rev.*, 2015, **115**, 8001–8037.
86 M. Mondal and A. K. H. Hirsch, *Chem. Soc. Rev.*, 2015, **44**, 2455–2488.
87 J. I. MacDonald, H. K. Munch, T. Moore and M. B. Francis, *Nat. Chem. Biol.*, 2015, **11**, 326–331.
88 K. A. McCarthy, M. A. Kelly, K. Li, S. Cambray, A. S. Hosseini, T. van Opijnen and J. Gao, *J. Am. Chem. Soc.*, 2018, **140**, 6137–6145.